Supporting Information

Kajal Panchal, Kaushalya Bhakar, Naresh Rajpurohit, and Dinesh Kumar*

School of Chemical Sciences, Central University of Gujarat, Kundhela, Vadodara 391107, Gujarat, India

*Corresponding author's email: dinesh.kumar@cug.ac.in

S13	EIS of CFS@NV-LDH at different applied voltage	S12

1. Experimental section

1.1 Material characterization

All chemicals and solvents were purchased from a commercial source and were free of further impurities. To evaluate the characteristics of as-synthesized materials, they are subjected to various analyses. Cu Kα (0.154nm) monochromatic radiation was employed with a Bruker AXS D8 focus for powder X-ray diffraction (P-XRD) to determine the crystallographic features. Scanning electron microscopy was used to analyse the structural configuration of the synthesized materials. The Brunauer-Emmett-Teller (BET) surface area of the composite and Barrett-Joyner-Halenda pore size distribution were analyzed by Quantachrome instruments. The oxidation state and binding energy of the developed material were studied in an N_2 atmosphere using a Thermo Fisher Nexsa XPS instrument. All electrochemical analyses were performed on a CHI920D workstation using a 3-electrode setup.

1.2 Electrochemical analysis in a 3-electrode system

The as-prepared binder-free, free-standing CFS@NV-LDH was carefully cut into 1 cm^2 pieces (~3 mg mass loading) and used as the working electrode, Ag/AgCl as the reference electrode, and a Pt wire as the counter electrode in a 3-electrode assembly. The mass loading was determined by measuring the weight difference of the nickel foam before and after the growth of the material using an analytical balance. The electrochemical analysis was performed using cyclic voltammetry (CV), galvanostatic charge-discharge (GCD), and electrochemical impedance spectroscopy (EIS) in a 2M KOH electrolyte solution.

1.3 Hybrid supercapacitor device fabrication

The free-standing CFS@NV-LDH electrode was used as the cathode, and for the anode, activated carbon, conducting carbon black, and PVDF binder were dispersed in NMP at an 8:1:1 ratio. Then, the slurry was drop-cast on a cleaned current collector. For assembly, the electrodes and cellulose paper were soaked in a 6 M KOH electrolyte and then assembled in a Swagelok cell.

1.4 Electrochemical calculations

The Specific capacitance (Cs), Energy Density (E_d), and Power Density (P_d) were calculated using the following equations (1), (2), and (3):

$$C_s(F\ g^{-1}) = \frac{I * \Delta t}{m * \Delta V} \qquad (S1)$$

Here, where C_s represents the specific capacitance, I refer to the applied current, m represents the mass loading of active material, ΔV is the operating potential window, and Δt is the discharge time (sec.).

$$E_d(\text{Wh}\ kg^{-1}) = \frac{C_s V^2}{7.2} \qquad (S2)$$

$$P_d(W\ kg^{-1}) = \frac{E_d * 3600}{\Delta t} \qquad (S3)$$

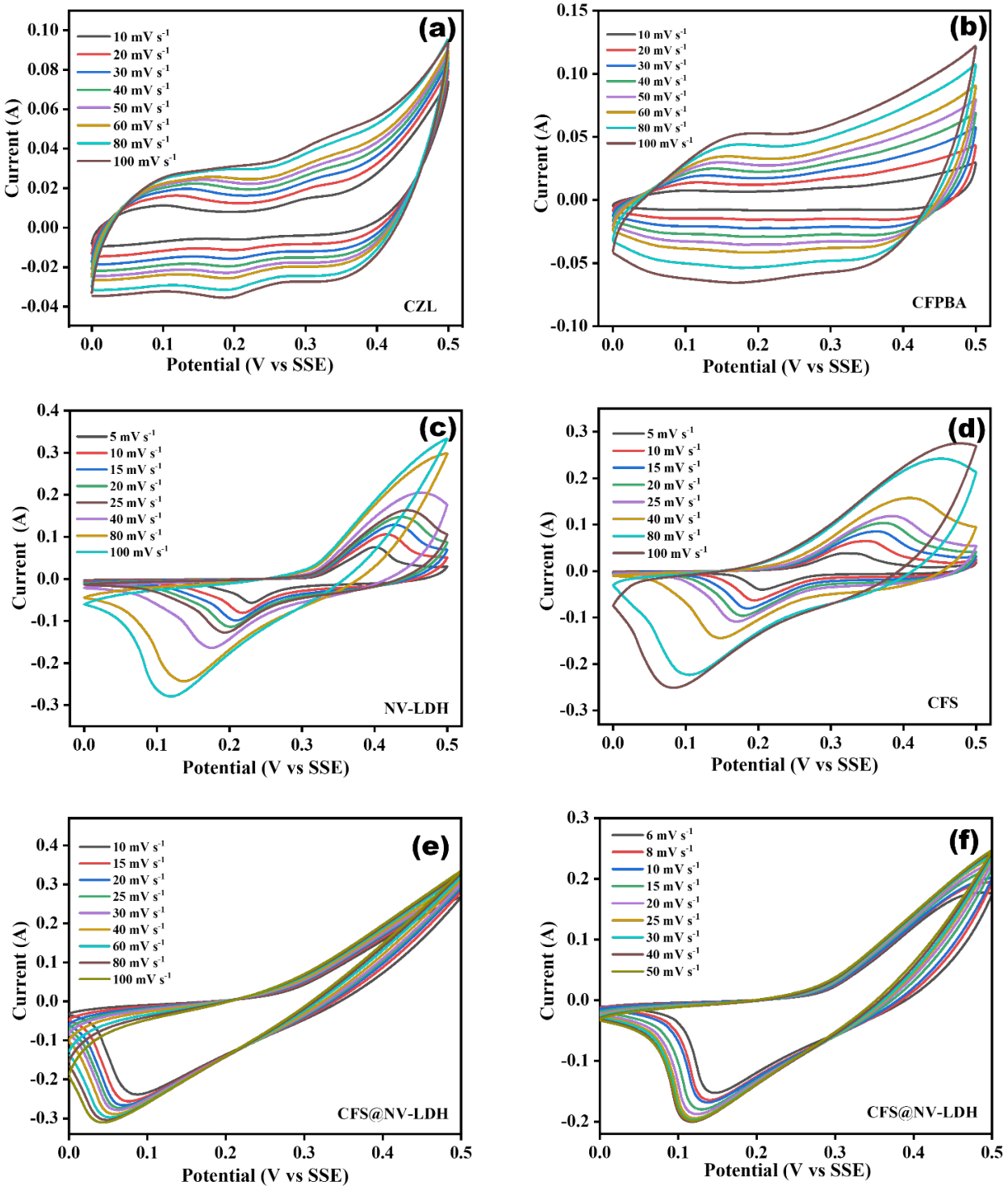

Fig. S1. CV plot of (a) CZL, (b) CFPBA, (c) NV-LDH, (d) CFS, (e & f) CFS@NV-LDH at variable scan rate

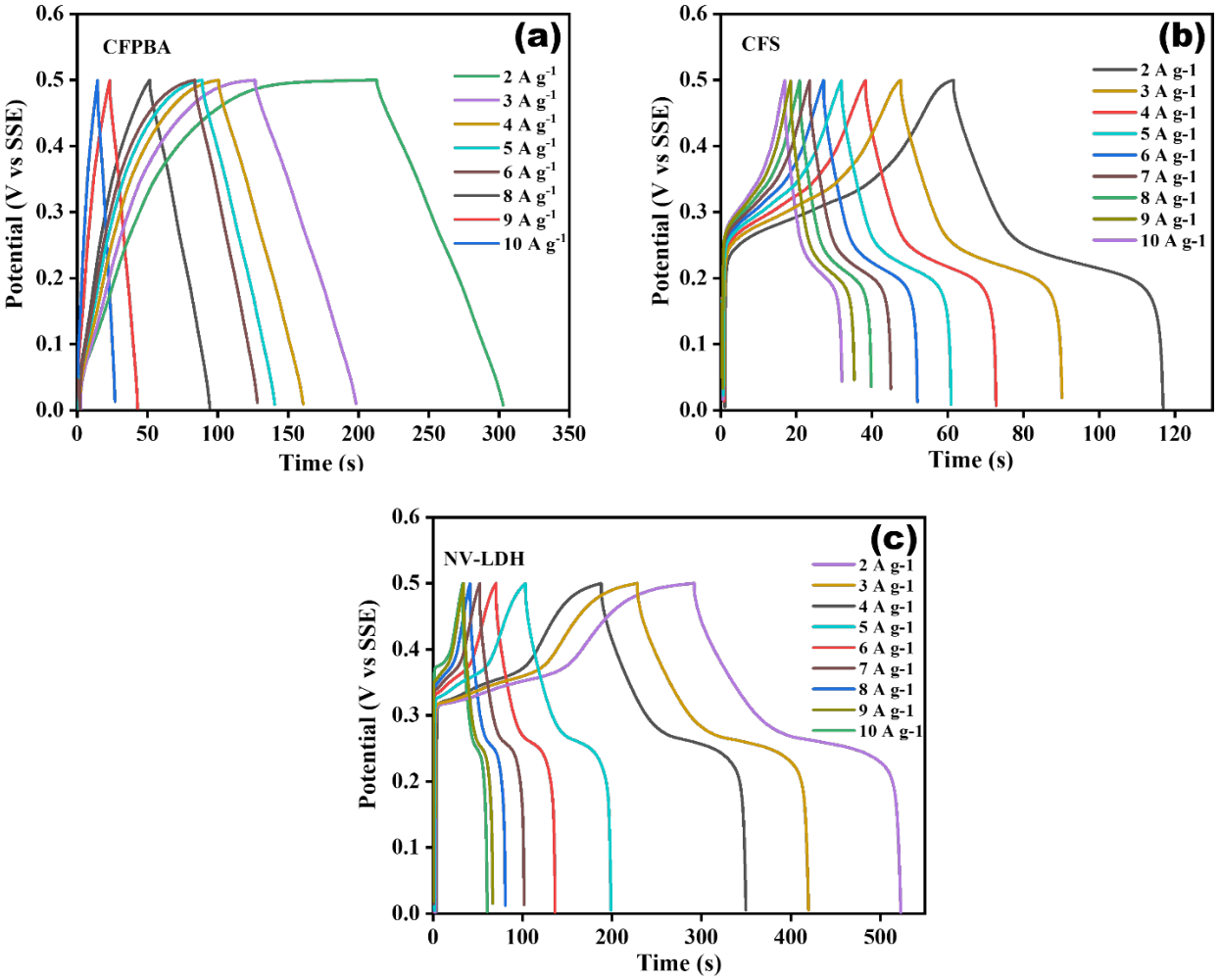

Fig. S2 GCD plot of (a) CFPBA, (b) CFS, (c) NV-LDH

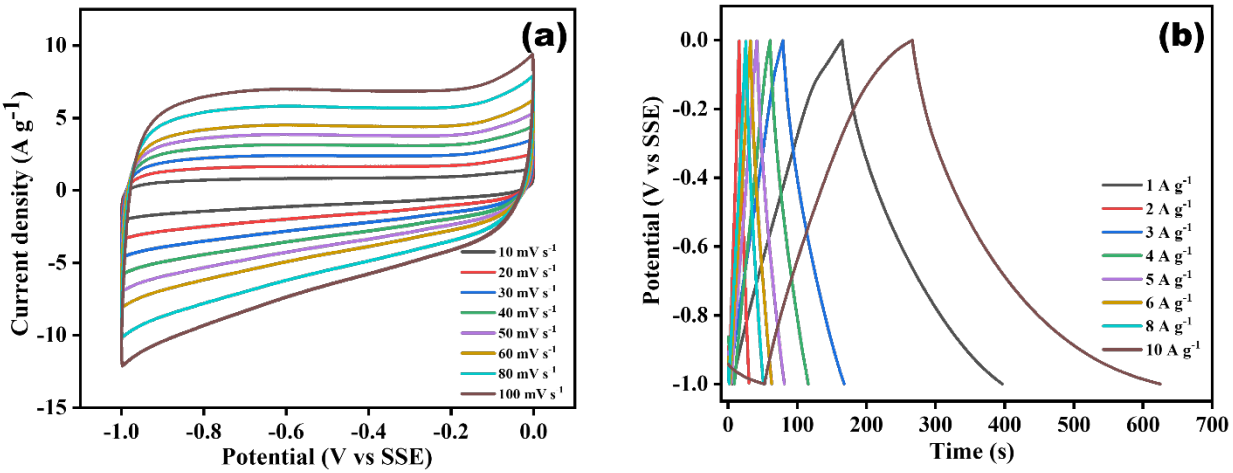

Fig. S3. (a) CV of activated carbon (AC) at variable scan rate, (b) GCD of AC at variable current density

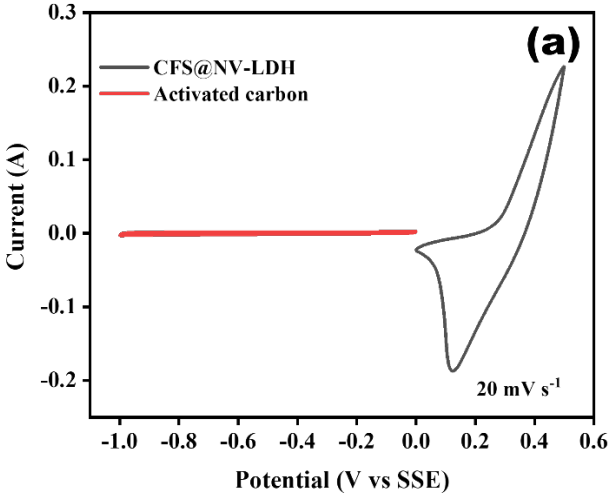

Fig. S4 Combined CV of CFS@NV-LDH and AC

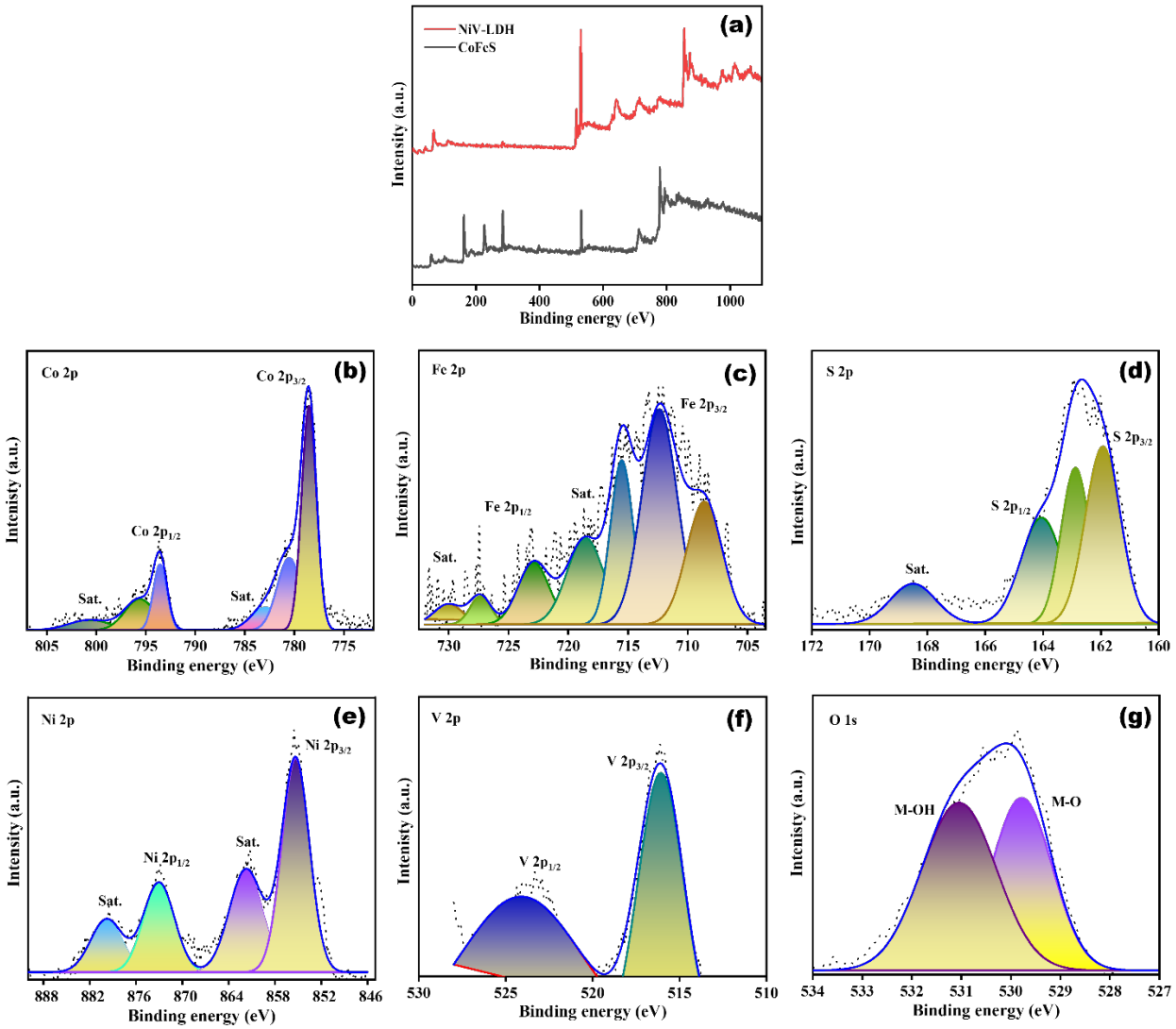

Fig. S5 (a) comparative survey spectra, **(b)** XPS spectrum of CFS Co 2p, **(c)** Fe 2p, **(d)** S 2p, **(e)** XPS spectrum of NV-LDH Ni 2p, **(f)** V 2p, **(g)** O 1s

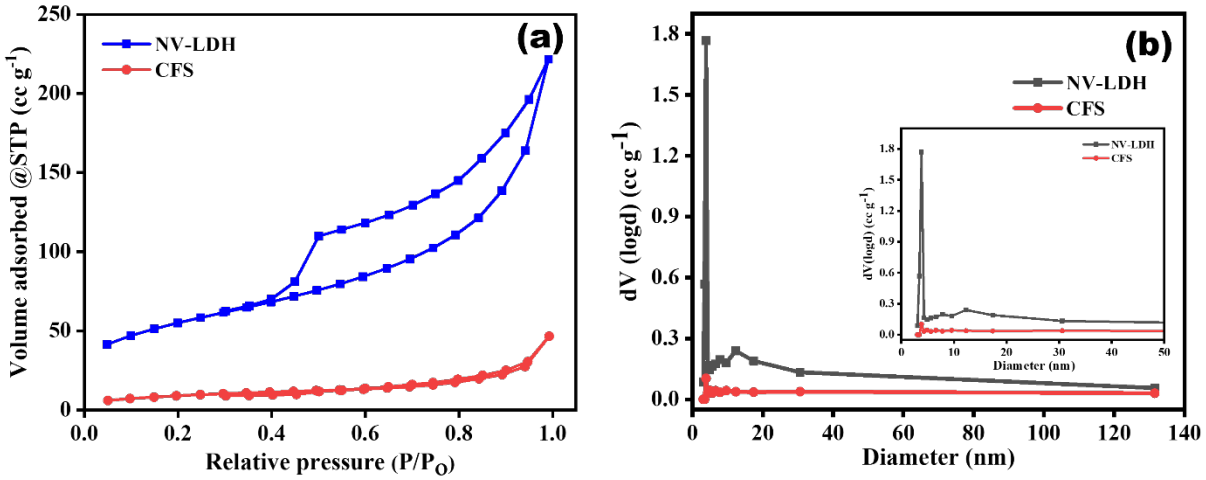

Fig. S6 (a) BET graph of CFS, and NV-LDH, **(b)** BJH graph of CFS and NV-LDH

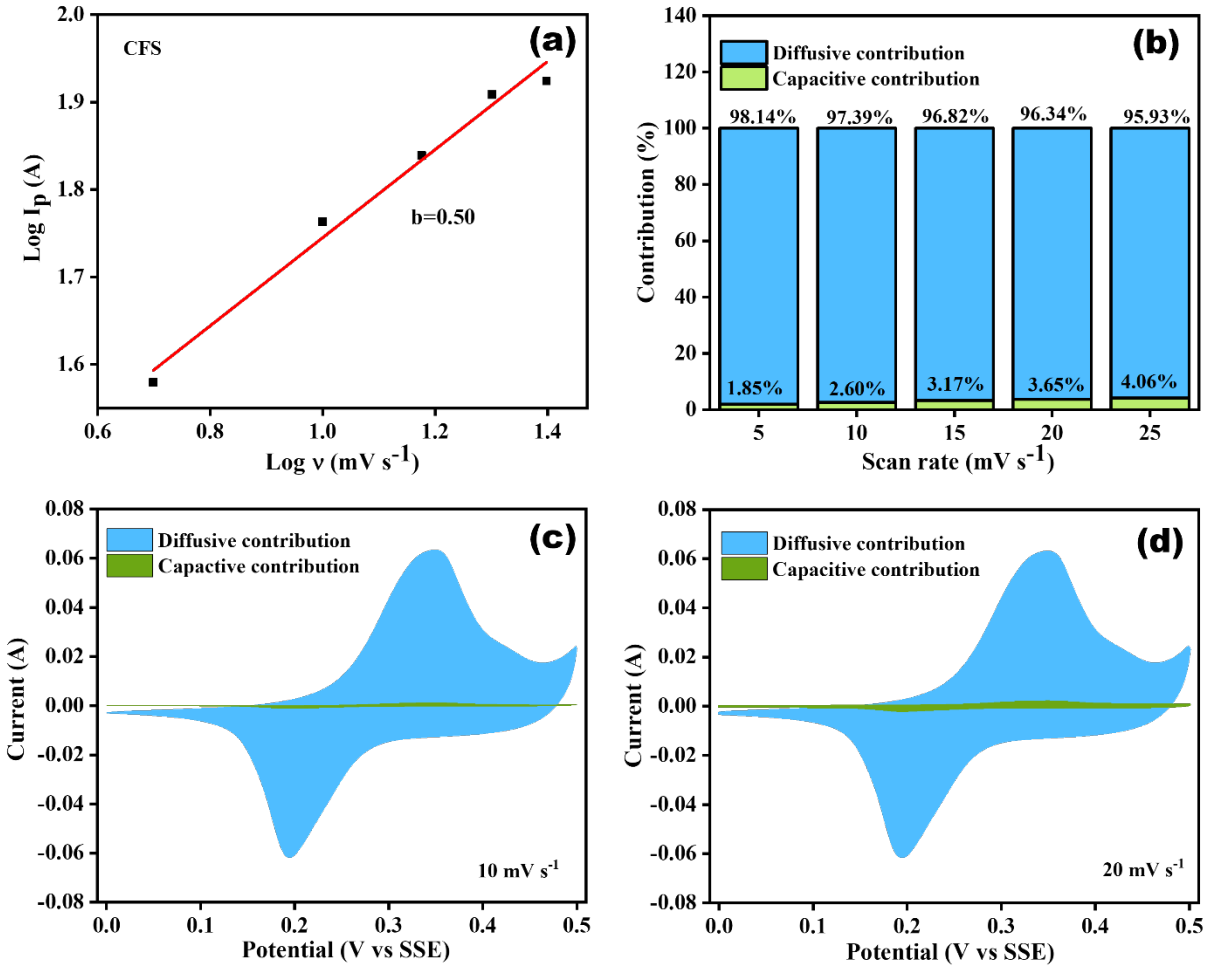

Fig. S7 Charge storage mechanism of CFS (a) Log Ip vs Log v plot, (b) diffusive and capacitive contribution at variable scan rate, (c) & (d) diffusive and capacitive contribution at 10 and 20 mV s^{-1} scan rate

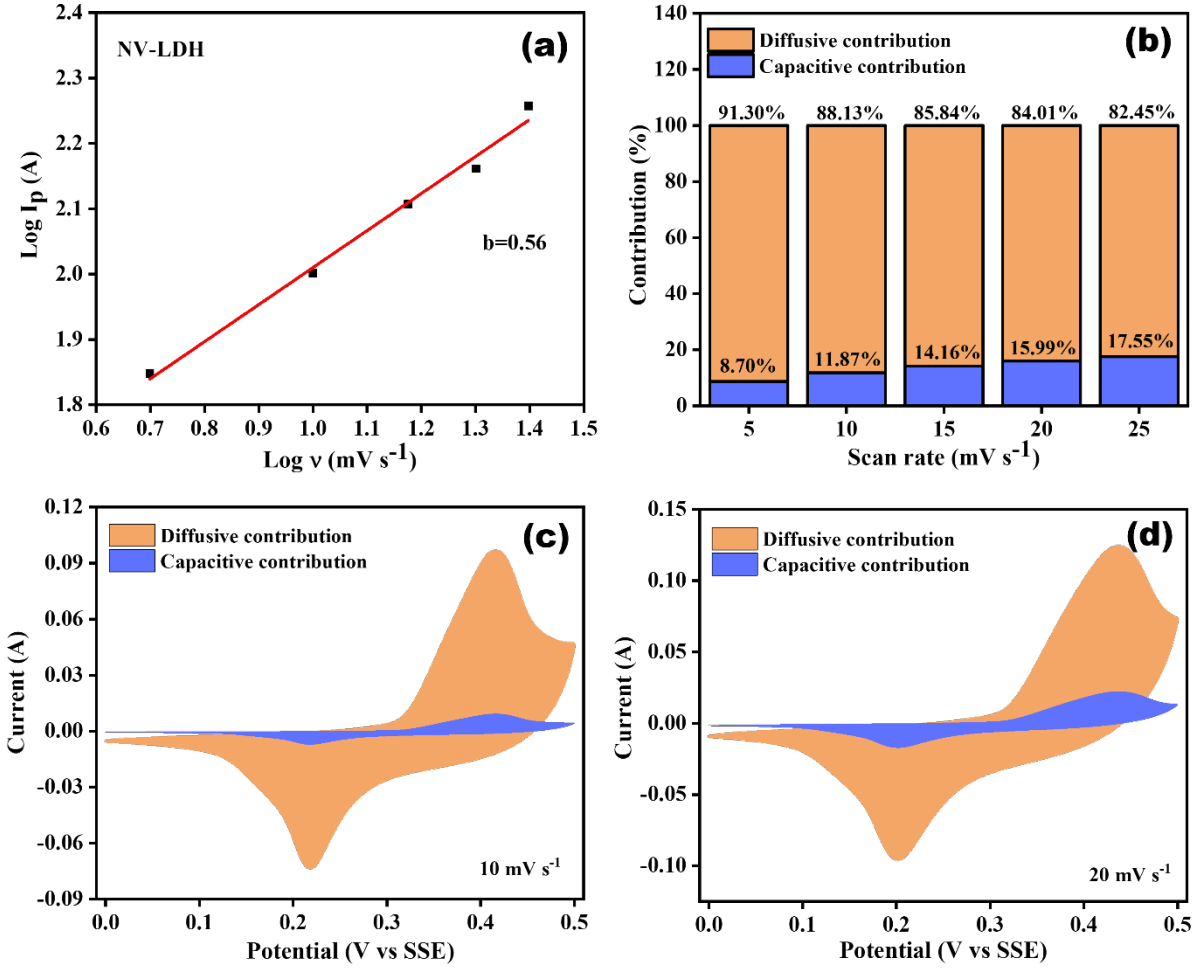

Fig. S8 Charge storage mechanism of NV-LDH (a) Log I_p vs Log v plot, (b) diffusive and capacitive contribution at variable scan rate, (c) & (d) diffusive and capacitive contribution at 10 and 20 mV s^{-1} scan rate

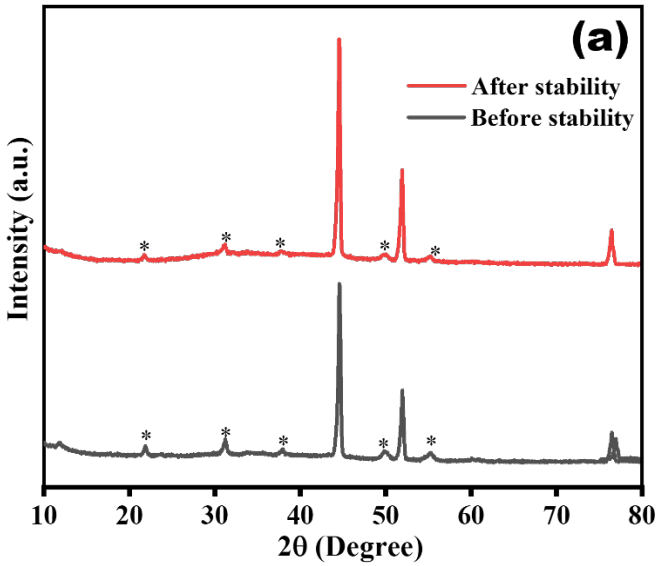

Fig. S9 (a) Post-stability XRD plot

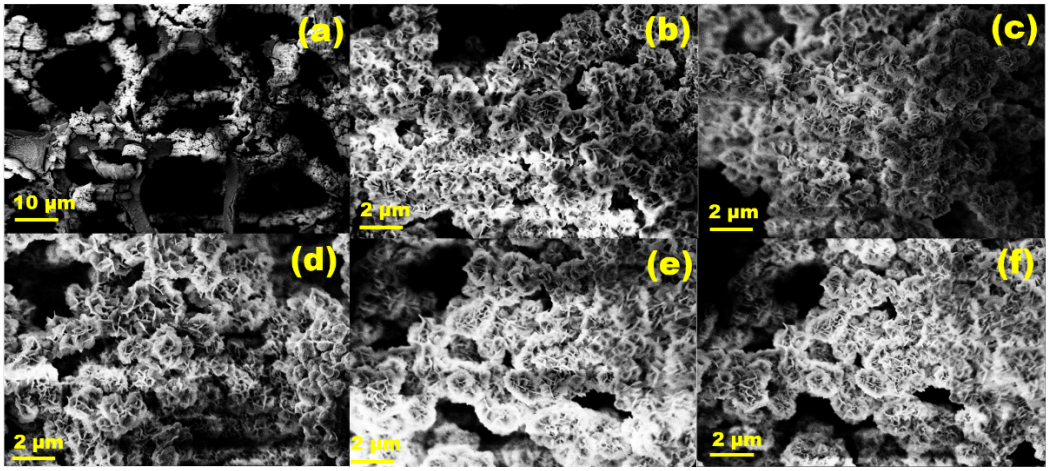

Fig. S10 (a-f) After stability SEM images of CFS@NV-LDH at different magnifications

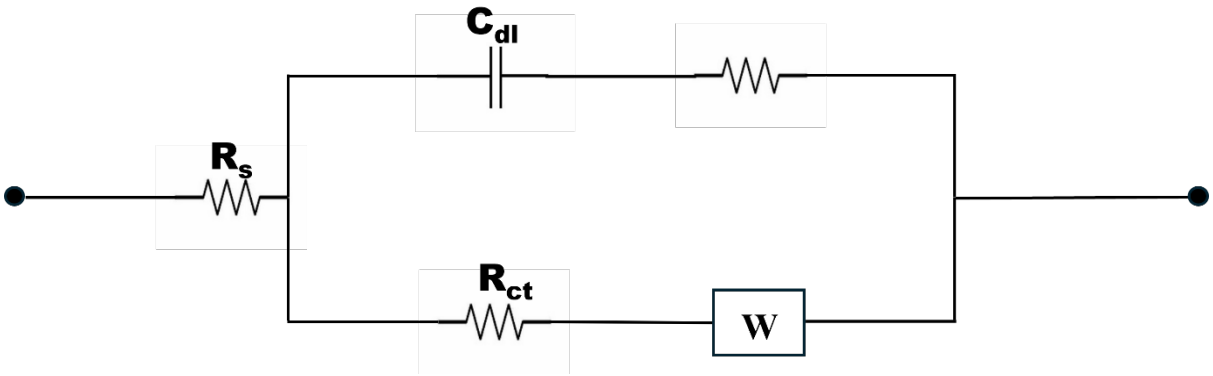

Fig. S11 EIS circuit diagram

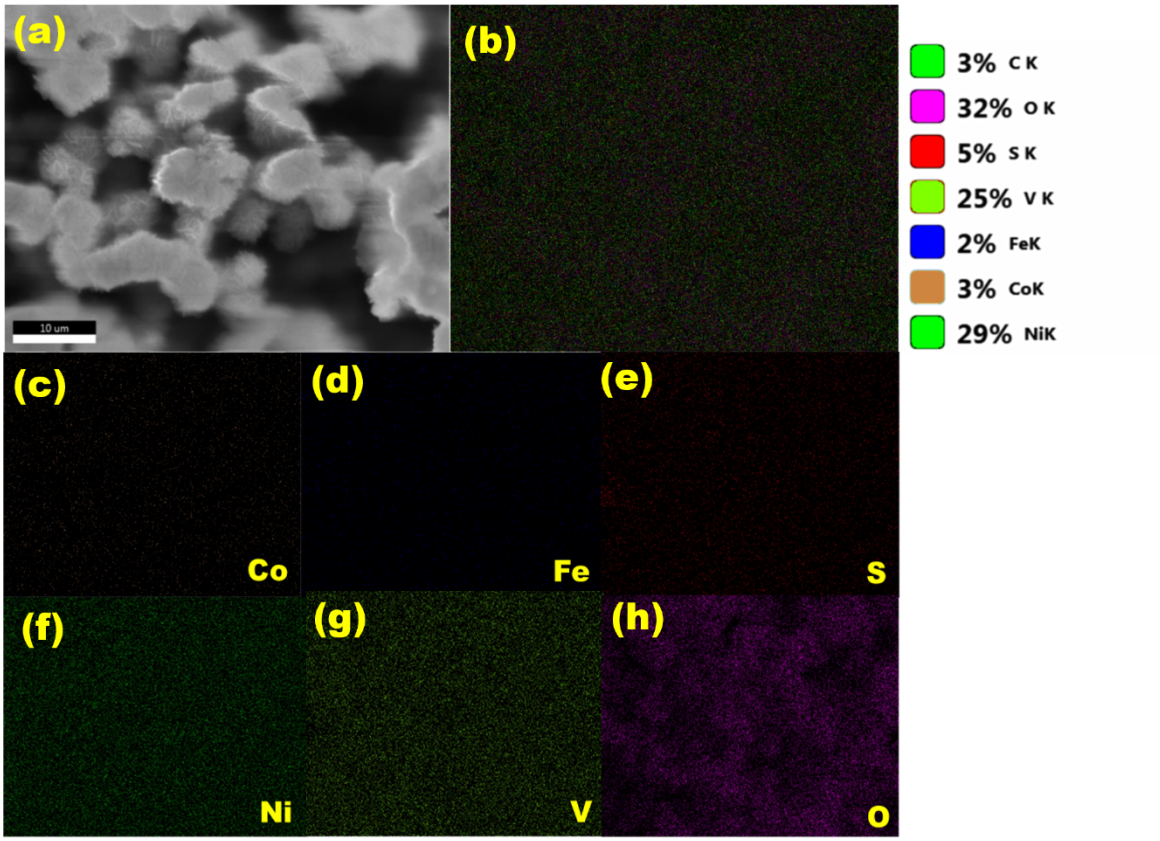

Fig.S12 EDX mapping of CFS@NV-LDH heterostructure

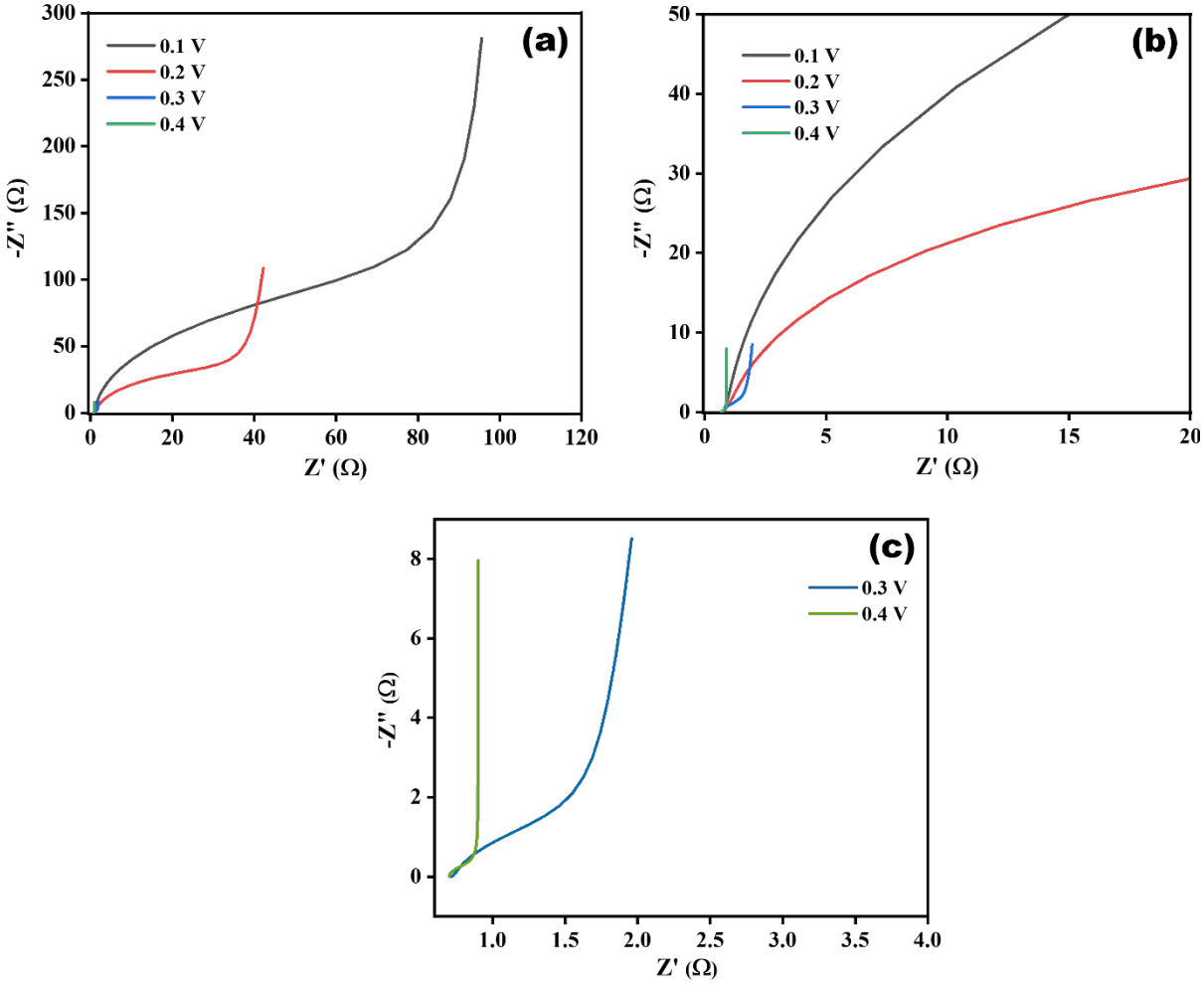

Fig. S13 EIS analysis of CFS@NV-LDH at different applied voltage (a), (b), &(c)